Marine and Petroleum Geology 72 (2016) 254–267

Contents lists available at ScienceDirect

Marine and Petroleum Geology

journal homepage: www.elsevier.com/locate/marpetgeo

Research paper

Geochemistry, origin and accumulation of natural gases in the deepwater area of the Qiongdongnan Basin, South China Sea

Baojia Huang [a, b], Hui Tian [a, *], Xushen Li [b], Zhenfeng Wang [b], Xianming Xiao [a]

[a] State Key Laboratory of Organic Geochemistry, Guangzhou Institute of Geochemistry, Chinese Academy of Sciences, Guangzhou 510640, China
[b] Zhanjiang Branch, CNOOC China Ltd, Zhanjiang 524057, China

ARTICLE INFO

Article history:
Received 11 April 2014
Received in revised form
1 February 2016
Accepted 4 February 2016
Available online 8 February 2016

Keywords:
Gas origin
Gas accumulation model
Deepwater area
Qiongdongnan basin
South China sea

ABSTRACT

The Qiongdongnan Basin, South China Sea has received huge thickness (>12 km) of Tertiary-Quaternary sediments in the deepwater area to which great attention has been paid due to the recent discoveries of the SS22-1 and the SS17-2 commercial gas fields in the Pliocene-Upper Miocene submarine canyon system with water depth over 1300 m. In this study, the geochemistry, origin and accumulation models of these gases were investigated. The results reveal that the gases are predominated by hydrocarbon gases (98%–99% by volume), with the ratio of $C_1/C_{1\text{-}5}$ ranging from 0.92 to 0.94, and they are characterized by relatively heavy $\delta^{13}C_1$ (−36.8‰ to −39.4‰) and δD_{CH4} values (−144‰ to −147‰), similar to the thermogenic gases discovered in the shallow water area of the basin. The $C_{5\text{-}7}$ light hydrocarbons associated with these gases are dominated by isoparaffins (35%–65%), implying an origin from higher plants. For the associated condensates, carbon isotopic compositions and high abundance of oleanane and presence of bicadinanes show close affinity with those from the YC13-1 gas field in the shallow water area. All these geochemical characteristics correlate well with those found in the shales of the Oligocene Yacheng Formation in the Qiongdongnan Basin. The Yacheng Formation in the deepwater area has TOC values in the range of 0.4–21% and contains type II_b–III gas-prone kerogens, indicating an excellent gas source rock. The kinetic modeling results show that the $\delta^{13}C_1$ values of the gas generated from the Yacheng source rock since 3 or 4 Ma are well matched with those of the reservoir gases, indicating that the gas pool is young and likely formed after 4 Ma. The geologic and geochemical data show that the mud diapirs and faults provide the main pathways for the upward migration of gases from the deep gas kitchen into the shallow, normally pressured reservoirs, and that the deep overpressure is the key driving force for the vertical and lateral migration of gas. This gas migration pattern implies that the South Low Uplift and the No.2 Fault zone near the deepwater area are also favorable for gas accumulation because they are located in the pathway of gas migration, and therefore more attention should be paid to them in the future.

1. Introduction

With an approximate area of 65,000 km^2, the Qiongdongnan Basin is one of the four petroliferous basins on the northern continental shelf of the South China Sea (Fig. 1a). The deepwater area (water depth greater than 300 m), located in the southern part of the basin, is about 45,000 km^2 and covers the central depression, including Ledong, Lingshui, Songnan, Baodao, Beijiao, and Changchang sags (Fig. 1b). Great attention has been paid to the deepwater area in recent years due to its thick sedimentary package and great potential for natural gas accumulation. More than three gas fields and a number of gas-bearing structures have been discovered since 1983 in the shallow water regions, including the Yacheng 13-1 giant gas field with the gas reserve of about 991 × 10^8 m^3 (3.5 TCF) in coastal estuarine sediments of the Oligocene Lingshui Formation (Huang et al., 2003b). Recently, the SS22-1 and SS17-2 gas fields were discovered in the submarine Central Canyon in the Lingshui Sag at a water depth over 1300 m, with an estimated gas resource of more than 1132 × 10^8 m^3 (4 TCF), showing great gas exploration potential in the deepwater area of this basin.

There have been several publications on the origin and accumulation of natural gases in the shallow water area of the

* Corresponding author.
E-mail addresses: tianhui@gig.ac.cn, huangbj@cnooc.com.cn (H. Tian).

http://dx.doi.org/10.1016/j.marpetgeo.2016.02.007
0264-8172/

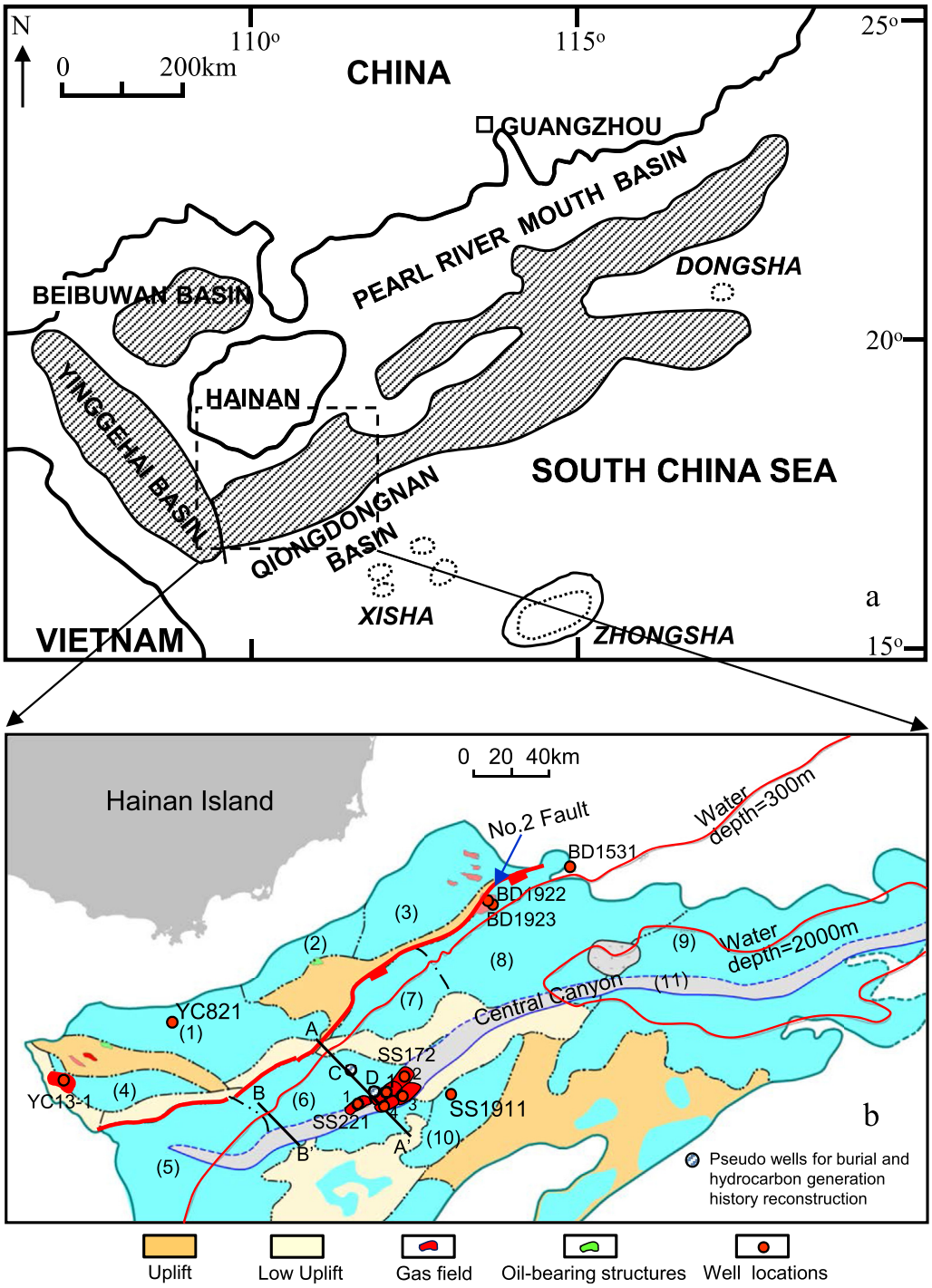

Fig. 1. Maps showing the location of Qiongdongnan Basin (a) and its deepwater part (b). (1) Yabei Sag; (2) Songxi Sag; (3) Songdong B Sag; (4) Yanan Sag; (5) Ledong Sag; (6) Lingshui Sag; (7) Songnan Sag; (8) Baodao Sag; (9) Changchang Sag; (10) Beijiao Sag; (11) Central Canyon. The term Uplift is used when there is no Paleogene strata in an area whereas the Low Uplift refers to an area where the stratigraphy is dominated by the Neogene and Quaternary strata, but with no or very thin Upper Oligocene strata.

Qiongdongnan Basin. The gases in Y13-1 gas field is believed to originate from the deeply-buried Oligocene Yacheng Formation source rocks in the Qiongdongnan Basin (Huang, 1999, 2003b; Xiao et al., 2006; Zhu et al., 2009). However, little information on the origin and accumulation of gases in the deep water part of the basin has been documented. In particular, the source rocks of the discovered gases remains unclear; thus the hydrocarbon potential in the deep water area has become one of the major concerns for further exploration. A detailed investigation into the geochemistry of gases will lead to a better understanding of their origins and help to predict gas distribution in the deep water areas of the Qiongdongnan Basin. For this purpose, this study investigated the geochemical characteristics and genetic origins of the gases in the SS22-1 and SS17-2 gas fields and provides an interpretation of their possible source rocks and accumulation models. This work will help to better define the favorable exploration areas and future drilling

targets in the deepwater area of the basin.

2. Geological setting

The Qiongdongnan Basin is located on the northern continental shelf of the South China Sea, a short distance to the east of the Yinggehai Basin and to the southwest of the Pearl River Mouth Basin (Fig. 1a). It is a Cenozoic rift basin developed on Mesozoic basement and contains a thickness of 6000–12,000 m Tertiary to Quaternary sediments (Zhu, 2007, Zhu et al., 2009).

The basin formed in response to the rifting associated with the opening of the South China Sea (Ru and Pigott, 1986). As illustrated in Fig. 2, the structural evolution of the basin can be divided into two stages: Eocene-Oligocene rift stage and Neogene-Quaternary post-rift thermal subsidence stage (Ru and Pigott, 1986; Gong and Li, 1997; Huang et al., 2003b; Zhu, 2007, 2009). Rifting commenced in the Eocene and finished around the Late Oligocene, leaving a series of half-graben or sags that are downthrown to the south and filled with lacustrine sediments. The Eocene strata in the basin have not been penetrated due to their deep burial in the sags and their absence in the uplifts. The Yacheng Formation was deposited during the early Oligocene and received mostly neritic

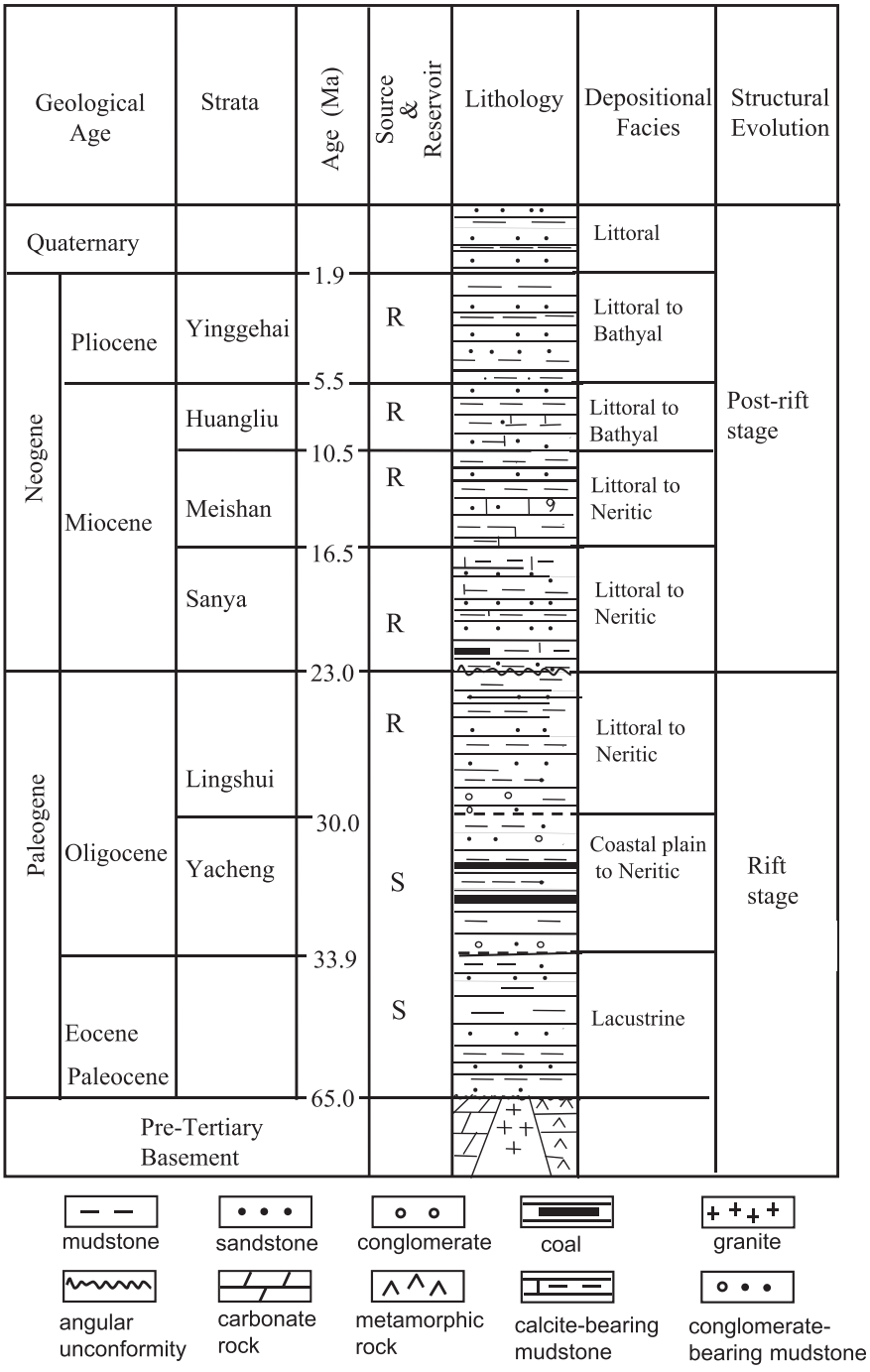

Fig. 2. Schematic stratigraphic columns of the Qingdongnan Basin. R = reservoir, S = source rock.

and coastal plain coal-bearing sediments. This coal-bearing formation is believed to be the main hydrocarbon source rock in the basin (Huang et al., 2003b; Xiao et al., 2006). Immediately above the Yacheng Formation are the littoral to neritic Lingshui Formation that contains about 50%–60% of sandstones over a large area, which form the most important reservoirs as well as the carrier beds for hydrocarbon migration.

Following the rifting stage, the Qiondongnan Basin experienced post-rift thermal subsidence until the present day and was filled with a thick sequence of marine sediments that are dominated by mudstones, with occasional turbidite channel and submarine fan sandstone bodies in the Miocene to Pliocene Sanya, Meishan, Huangliu and Yinggehai Formations. These sandstones form another set of favorable reservoirs. It is noteworthy that the Central Canyon System, a large axial submarine canyon in the Qiongdongnan Basin, was developed during the Neogene and is sub-parallel to the continental slope with an NE–NEE trend (Gong et al., 2011; Su et al., 2014). Mud diapirs developed beneath the canyon and the basin center area (Fig. 3), and the diapiric faults can act as preferential pathways for the upward migration of natural gases from the deep sources into the Miocene sandstone bodies. The major tectonic control in this area is associated with SW/NE extensional faults that have controlled the deposition of both the Paleogene and Neogene sediments (Zhu et al., 2009).

The Qiongnandong Basin is characterized by high sedimentation rates of up to 1.2 mm/year (Zhu, 2007, Zhu et al., 2009) and a high present-day geothermal gradient of up to 39–45 °C/km (Shi et al., 2014). As a result of rapid sediment loading, overpressure associated with undercompaction is a common phenomenon at depths greater than 3300 m beneath the sea surface throughout the central Qiongdongnan Basin, especially in the deepwater area. The combination of overpressure and high paleo-geothermal gradient, together with faulting or diapirism, has significantly influenced the generation, migration and accumulation of natural gases in the basin (Zhu et al., 2009).

Natural gas discoveries in the shallow water area of the Qiongdongnan Basin are mainly in the YC13-1 gas field, and the YC13-4 and YC 13-6 gas-bearing structures, northwest of the Yanan Sag (Fig. 1b). The BD19-2 gas pool is located near the No.2 Fault (close to the deepwater area) in the northwest of Baodao Sag, and produces gas from the Upper Oligocene marine sandstones of Lingshui Formation in the depth ranging from 3750 m to 5201 m beneath the sea surface. The recently discovered SS22-1 and SS17-2 gas fields are located in the Lingshui Sag with a water depth greater than 1300 m. The pay formations are stacked turbidite sandstone packages within the Miocene–Pliocene submarine Central Canyon (Fig. 1b). The SS22-1 and SS17-2 traps were formed after the deposition of muddy sediments in the lower part of Yinggehai Formation (early Pliocene); the reservoir rocks, overlying the Oligocene coal-bearing Yacheng Formation, are buried 3300–3500 m beneath the sea surface and almost hydrostatically pressurized with formation pressure coefficients (Cp, the ratio of measured formation pressure to hydrostatic pressure) in the range of 1.0–1.2.

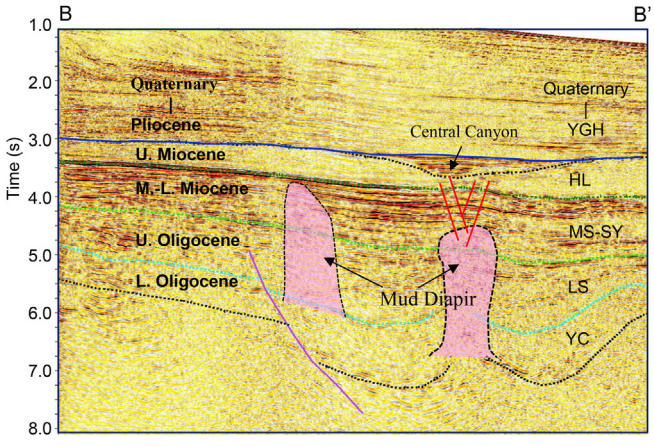

Fig. 3. Seismic profile through the Central Submarine Canyon in the Qiongdongnan Basin, showing the diapir piercing zone and associated faults. The location of the section is shown in Fig. 1b. YGH-Yinggehai formation; HL-Huangliu Formation; MS-Meishan Formation; SY-Sanya Formation; LS-Lingshui Formation; YC-Yacheng Formation.

3. Samples and methods

3.1. Samples

About 220 cutting and core samples from 6 wells were collected for TOC and Rock–Eval analysis, and natural gas samples were collected during drill stem tests and module formation tests for geochemical and isotopic analysis (Table 1).

3.2. TOC, Rock-Eval and macerals

The total organic carbon (TOC) was measured by LECO CS-200 analyzer after the samples were treated by hydrochloric acid to remove the carbonates. Rapid pyrolysis was carried out on original samples using a Vinci Technology Rock-Eval 6 instrument to obtain the quantity of free hydrocarbons present in the sample (S_1 peak) and the amount of hydrocarbons generated during the thermal cracking of kerogen in the rocks (S_2 peak). The sum of S_1 and S_2 indicates the current hydrocarbon potential of a rock sample.

Maceral analysis was performed with a Leica MPV microscope using reflected white and fluorescent light. An oil immersion objective (50 × magnification) was used. A total of 500 points per polished block were counted using the single scan method (Taylor et al., 1998). The abundance of individual maceral was expressed as the percentage of total particle abundances (% PAs).

3.3. Gas geochemistry, stable carbon and hydrogen isotopes and helium isotope

The gas samples were analyzed using a Hewlett Packard 5890 II gas chromatograph equipped with a thermal conductivity detector. The gas chromatography (GC) employed a HP-5 fused silica capillary column (50 m × 0.32 mm i.d. × 0.25 μm film thickness) and helium carrier gas. The gas was injected at a column temperature of 50 °C and held for 2 min, after which the oven was subsequently heated to 180 °C at a rate of 4 °C/min and held at 180 °C for 15 min. In addition, a part of the gases was analyzed directly using gas chromatography for the determination of C_{2-7} range hydrocarbon parameters. The carbon and hydrogen isotopic compositions were measured on a Finnigan-MAT251 mass spectrometer. Isotopic values are reported in per mil (‰) relative to Peedee belemnite (PDB) standard for carbon and relative to standard mean ocean water (SMOW) for hydrogen. The analytical precisions for carbon and hydrogen isotope measurements are ±0.2‰ and ±3‰, respectively. The $^3He/^4He$ measurements were conducted using a VG-5400 static-vacuum noble gas mass spectrometer, with an analytical precision of ±0.6%. The $^3He/^4He$ ratios of gas samples were compared to the $^3He/^4He$ ratios of air to yield the R/Ra ratios (Oxburgh et al., 1986).

Table 1
Chemical and stable carbon isotopic compositions of natural gases produced from the Qiongdongnan Basin[a].

Samples no.	Depth	Reservoir	N_2	CO_2	C_1	C_{2-5}	C_{6+}	C_1/C_{1-5}	$\delta^{13}C_1$	$\delta^{13}C_2$‰	$\delta^{13}C_3$	$\delta^{13}C_{CO2}$‰	δD_{C1}	R/Ra
	(m)		%	%	%	%	%		‰		‰		‰	
SS1721-1	3306	HL	0.68	0.45	92.51	6.14	0.24	0.94	−36.8	−23.5	−22.0	−16.6	nd	nd
SS1721-2	3324	HL	0.62	0.21	93.25	5.79	0.14	0.94	−36. 8	−23.6	−22.2	−17.8	nd	nd
SS1721-3	3366	HL	0.63	0.46	92.69	5.93	0.28	0.94	−37.3	−23.8	−21.9	−16.3	nd	nd
SS1721-4	3368	HL	0.61	0.52	92.56	6.04	0.27	0.94	−36.8	−24.1	−21.6	−15. 7	nd	nd
SS1721-5	3321–3351	HL	0.26	0.62	93.00	5.97	0.16	0.94	−37.3	−24.1	−22.3	−9.2	nd	nd
SS1722-1	3329	HL	1.66	0.70	91.68	5.90	0.02	0.94	−38.2	−23.7	−21.8	−20.7	nd	nd
SS1722-2	3331	HL	0.84	0.06	93.04	6.25	0.25	0.93	−37.4	−24.2	−23.2	−18.1	nd	nd
SS1723-1	3407	HL	2.56	0.53	89.45	7.21	0.25	0.93	−38.0	−25.3	−23.8	−19.7	nd	nd
SS1724-1	3251	HL	0.58	0.20	90.97	7.68	0.57	0.93	−39.0	−25.4	−23.7	nd	nd	nd
SS1724-2	3445	HL	0.66	0.61	90.31	7.89	0.54	0.93	−38.4	−25.8	−24.6	−14.4	nd	nd
SS2211-3	MDT3	HL	0.55	0.32	91.53	7.2	0.39	0.93	−39.2	−26.0	−24.1	−9.6	−144	nd
SS2211-4	MDT4	HL	0.54	0.3	91.7	7.16	0.3	0.93	−39.0	−25.9	−23.8	−9.2	−147	nd
SS2211-5	MDT5	HL	0.56	0.31	91.12	7.47	0.55	0.92	−39.4	−26.2	−24.3	nd	−145	nd
SS2211-6	MDT6	HL	0.55	0.31	91.16	7.48	0.5	0.92	−39.2	−26.2	−23.8	nd	−146	nd
SS2211-7	MDT7	HL	0.57	0.32	91.37	7.28	0.47	0.93	−38.8	−26.0	−23.7	−8.5	−147	nd
BD1922-2	5100	LS3	1.52	81.56	16.06	0	0	1.00	nd	nd	nd	−6.9	nd	4.25
BD1922-1	5127.6	LS3	1.85	87.52	9.79	0.74	0	0.93	−38.8	nd	nd	−7.50	nd	6.25
BD1923-2	3911	LS2	6.28	4.42	79.7	8.29	0.12	0.91	−36.0	−30.4	−28.6	−6.2	nd	3.87
BD1923-1	3934.5	LS2	3.84	18.72	72.93	3.73	0.13	0.95	−35.2	−30. 7	−28.6	−4.3	nd	2.66
[b]YC1311-3	3573.8–3586.3	LS	0.72	9.6	85.03	3.74	0.91	0.96	−35.7	−25.2	−24.2	−4.9	nd	nd
YC1311-2	3658.8–3701.9	LS	1.04	10.79	84.18	3.36	0.63	0.96	−35.5	nd	nd	nd	nd	nd
YC1311-1	3728.9–3759.8	YC	4.65	0.17	89.81	4.95	0.37	0.95	−34.4	nd	nd	nd	nd	nd
YC1312-5	3708.8–3725.6	LS	1.02	8.1	87.22	3.15	0.51	0.95	−36.9	−24.0	nd	−5.1	nd	nd
YC1312-4	3771.6–3849.6	LS	0.3	10.1	88.52	0.98	0.1	0.99	−34.8	−24.6	nd	nd	−121	nd
YC1312-3	3888.6–3907.5	LS	0.1	11.5	86.53	1.81	0.06	0.98	−35.1	nd	nd	nd	nd	nd
YC1314-4	3842–3870.9	LS	1.23	6.7	85.71	6.09	0.27	0.93	−37.8	−26.0	−24.5	−8.3	−142	nd
YC1314-2	3943.5–3961.8	LS	0.81	7.92	85.98	4.39	0.90	0.95	−36.9	−26.2	−25.2	−6.1	nd	nd
YC1313-5	3788.7–3817.3	LS	1.04	8.54	83.22	6.98	0.22	0.92	−39.4	−26.5	−25.0	−7.7	−127	nd
YC1316-3	3774.9–3817.6	LS	0.93	4.99	85.5	8.34	0.24	0.91	−39.9	−26.8	−25.4	−10.3	−142	nd

[a] HL, Huangliu Formation(Upper Miocene); LS, Lingshui Formation(Upper Oligocene); YC, Yacheng Formation(Lower Oligocene); b: data from Huang et al., 2003b and Zhu et al., 2009; nd = no data.

Table 2
Kinetic parameters of methane carbon isotope fractionation for the Yacheng Formation source rock sample[a].

Sample	$^{13}A/^{12}A$	β_L (cal/mol)	β_H (cal/mol)	μ (cal/mol)	σ (cal/mol)	$\delta^{13}C_{ini}$(‰)
Oligocene Yacheng mudstone	1.02	23.14	80.36	53387	3043.05	−25.9

[a] $^{13}A/^{12}A$, the ratio value of frequency factors of isotopically heavy methane and isotopically light methane; β_L, the lowest value of activation energy differences; β_H, the highest value of activation energy differences; μ, the mean value of the Sigmoid function; σ, the variance of the Sigmoid function; $\delta^{13}C_{ini}$, the carbon isotopic values of methane precursors (See details in Tang et al., 2000).

3.4. GC–MS and biomarkers

Gas chromatography-mass spectrometric (GC–MS) analyses of the saturated fractions of condensates and dichloromethane extracts of source rocks were carried out using a Thermo DSQ II-Trace/MS220-5327. The chromatograph was equipped with a programmable temperature injection system and a fused silica column (30 m × 0.25 mm i.d. and 0.25 μm film thickness). The oven temperature was programmed from 50 °C to 300 °C at 2.5 °C/min and held for 30 min at the final temperature. High-purity helium was used as carrier gas at a flow rate of 1.2 ml/min. Samples were routinely analyzed in full scan mode (*m/z* 50–580). Biomarker identification was based on the comparison of mass spectra and GC retention time with previous documents. In the process of analysis, the blank experiment was performed to ensure that there are no contaminants or residues of previous samples.

3.5. Pyrolysis experiments and kinetic modeling of gas generation

Anhydrous and closed pyrolysis experiment was conducted using sealed gold tubes (Hill et al., 2007). A typical immature mudstone sample (side wall core with Ro = 0.6% and Tmax = 435 °C) was collected from the Yacheng Formation in the Qiongdongnan Basin. The sample has a TOC content of 1.23% with a hydrogen index of 190 mg/gTOC. Concentrated kerogen, isolated from the selected source rock sample, has a hydrogen index of 197 mg/gTOC with a Tmax value of 436 °C; kerogen splits were loaded into gold tubes (9 mm o.d. × 60 mm length) and heated from room temperature to 250 °C within 12 h and then programmed to designed temperatures between 300 °C and 600 °C at two heating rates of 2 °C/h and 20 °C/h, respectively. A constant confining pressure of 50 MPa was used throughout the pyrolysis experiment with an error of less than 2 MPa. The gaseous pyrolysates (C_{1-5}) were analyzed by GC and quantified using an external standard. The GC employed a Poraplot Q capillary column (30 m × 0.25 mm × 0.25 μm) and helium as carrier gas. The oven temperature for the hydrocarbon gas analysis was initially held at 70 °C for 6 min, ramped from 70 to 130 °C at 15 °C/min, from 130 to 180 °C at 25 °C/min, and then held at 180 °C for 4 min. The carbon isotopic compositions of pyrolysate gases were measured on a Delta Plus XL gas chromatograph–isotope ratio mass spectrometer (GC–IRMS). The GC was equipped with a Poraplot Q capillary column (30 m × 0.32 mm × 0.25 μm). Helium was used as carrier gas. The samples were injected at an initial temperature of 50 °C (held for 3 min), after which the oven was heated to 190 °C at a rate of 15 °C/min and held at that temperature for 15 min.

Based on the gas yields at the two heating rates, the kinetic parameters of gas generation, i.e. the activation energy and the frequency factor, were calculated with assumption that the gas generation can be described by a set of parallel first order reactions using the commercial software Kinetics 2005. The kinetic parameters for methane carbon isotope fractionation were fitted using the method of Tang et al. (2000).

4. Results and discussion

4.1. Geochemistry of natural gases

The gases from the SS22-1 and the SS17-2 gas fields comprise approximately 91.2–92.9% methane, 5.9–7.5% C_{2+} hydrocarbons and 0.78–3.09% nonhydrocarbon gases (N_2 and CO_2). Both the ratios of C_1/C_{1-5} by volume ranging from 0.92 to 0.94 and the $\delta^{13}C_1$ (−36.8 to −39.4‰, Table 1) indicate a thermogenic origin (Schoell, 1983; Tissot and Welte, 1984). The $\delta^{13}C_2$ values range from −23.5‰ to −26.2‰ and are similar to those of the gases from the YC 13-1 gas field (Table 1). Based on the gas data from the Chinese petroliferous basins, Xu and Shen (1996) proposed that the plot of $\delta^{13}C_1$ vs $\delta^{13}C_2$ could be used to identify the genetic types of natural gases. As illustrated in Fig. 4, the gases from both SS22-1 and SS17-2 gas fields plot within the coal-associated sector, similar to gases from the YC 13-1 gas field, indicating that the SS22-1 and SS17-2 gas fields probably have similar gas sources as the YC13-1 gas field, whose gas is believed to originate mainly from the Oligocene coal-bearing source rocks, such as Yacheng Formation (Huang et al., 2003b). This interpretation is also supported by the high contents of isoparaffins. As shown in Fig. 5, the composition of C_{5-7} light hydrocarbons associated with these gases is dominated by isoparaffins (35–65%), with a moderate content of normal paraffins (25–50%) and a small amount of cycloalkanes (5–25%). Although the relative enrichment of isoparaffins can be caused by the maturation of organic matter, it has been well documented that gas-prone source rocks of Type III kerogen or coaly origin usually produce more isoparaffinic components than oil-prone source rocks (Leythaeuser et al., 1979; Dai, 1993; Wang et al., 2008). For the thermal maturity evaluation of natural gas resulting from coaly source rocks with type III kerogen, Cramer et al. (1998) reported a curve of the $\delta^{13}C_1$ evolution with thermal maturity for coal gas and illustrated that a carbon isotope fractionation of 10‰ corresponds to a Ro value of approximately 2.0%. The larger the carbon isotope fractionation, the lower the thermal maturity. The bulk carbon isotopes of coaly Oligocene source rocks with type III kerogen in our study area are mainly in the range between −27.9 and −27.0‰ (Chen et al., 1998; Zhu, 2007), therefore the $\delta^{13}C_1$ range between −36.8 and −39.4‰, along with the low dryness index (0.92–0.94) for the natural gas analyzed here in our study indicates a thermal maturity level with Ro value of around 2.0%.

The CO_2 gases in and near the deepwater areas can be divided into two genetic types based on their contents and stable carbon

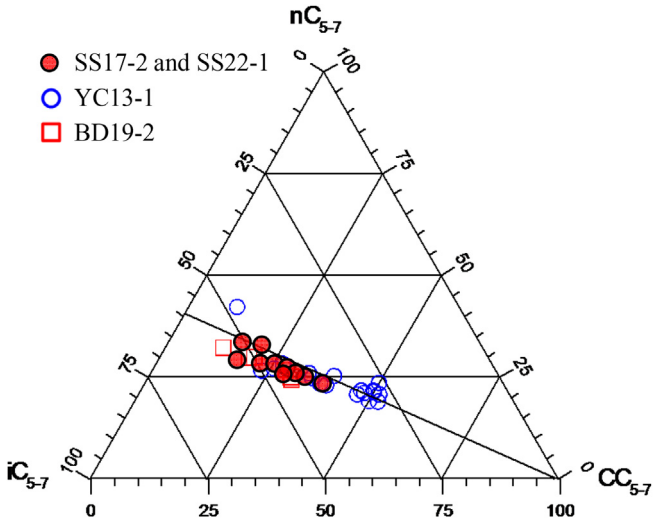

Fig. 5. Tertiary plot of C_{5-7} light hydrocarbons associated with the natural gases collected from the Qiongdongnan Basin, showing the correlations between the gases from the SS17-2+SS22-1(deepwater area) and the YC13-1(shallow water area). nC_{5-7}: C_{5-7} normal paraffins; iC_{5-7}: C_{5-7} isoparaffins; CC_{5-7}: C_{5-7} cycloalkanes.

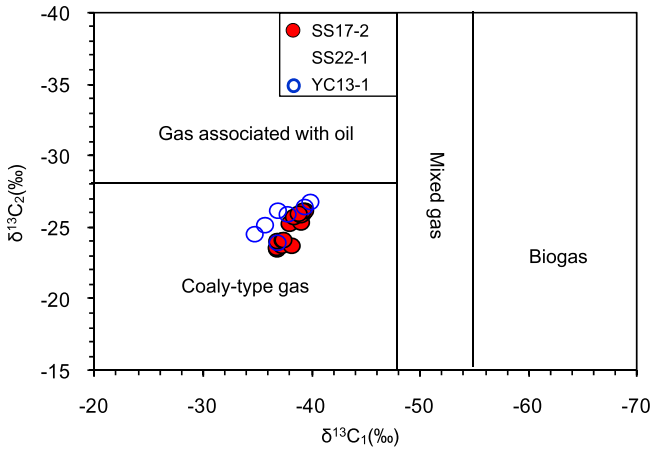

Fig. 4. Cross plot of $\delta^{13}C_1$ vs. $\delta^{13}C_2$ for gas samples collected from the Qiongdongnan Basin, showing the genetic types of gases from the SS22-1 and SS17-2 (deepwater area) and YC13-1gas fields (shallow water area). The boundary lines are taken from Xu and Shen (1996).

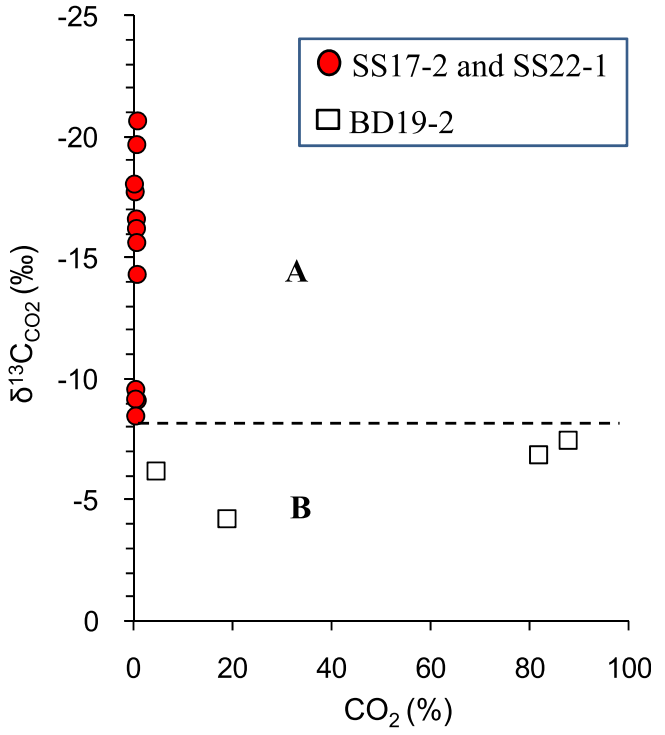

Fig. 6. Classification of CO_2 gas in the SS22-1 and SS17-2, and the BD19-2 gas pools in the Qiongdongnan Basin. (A) CO_2 generated from organic matter, (B) CO_2 derived from mantle.

isotope values (Fig. 6). The CO_2 from both the SS22-1and SS17-2 fields are low in content (0.06–0.70% by volume) and characterized by $\delta^{13}C_{CO2}$ values ranging from −20.7‰ to −8.5‰, indicating a predominant organic origin with a minor inorganic contribution. Three of four gas samples from the BD19-2 gas pool, however, have CO_2 contents of 18.72–87.52% and are characterized by more positive $\delta^{13}C_{CO2}$ values ranging from −6.9‰ to −4.3‰, and the R/Ra ratios for helium associated with these CO_2 gases range from 2.66 to 6.25 (Table 1), similar to those of mantle- and magmatic-derived CO_2 gases in eastern China basins (Dai et al., 1996; Zhang et al., 2008). Since these CO_2 gases are located in deeper reservoirs that are connected with deeply buried basement faults, they are interpreted to be of mantle origin, migrating into the reservoirs that are cut through by No.2 Fault. Stratigraphically, the CO_2-rich gases usually occur in the deeper Oligocene Liushui-3 Formation reservoirs, whereas hydrocarbon-rich gases are discovered mainly in shallower reservoirs of the Oligocene Liushui-2 Formation (Table 1, Fig. 1b). For example, the gases from the well BD1923, which is farther from the No. 2 Fault, contain 76.8–88.1% hydrocarbon gases with a small amount of CO_2 (1.19–18.72%). This suggests that the CO_2 risk could be significantly reduced in the deepwater area where the reservoirs are far from the No. 2 Fault.

4.2. Geochemistry of possible source rocks

Possible source rocks in the Qiongdongnan Basin are distributed within both the Oligocene and the Eocene strata (Huang, 1999; Huang et al., 2003b; Xiao et al., 2006; Zhu, 2007). At present, the Eocene source rocks have not been penetrated due to their absence in the uplifts of the basin, and therefore their TOC and hydrocarbon potential data are not available for this study. The Rock-Eval results of the Yacheng Formation source rocks are summarized and presented in Fig. 7. The Yacheng Formation is mainly present in the Paleogene half grabens of the Qiongdongnan Basin. The coal-bearing sequence, deposited in a coastal plain setting, has a total thickness up to 2500 m in the central Yacheng Sag (Zhu, 2007). Drilling results in shallow water areas show that the Yacheng Formation in this area is comprised of 40–70% mudstones whose total thickness is in the range of 483 m to 910 m (Zhu, 2007). Among them, the carbonaceous mudstones and coals are relatively thin with an aggregate coal layer thickness of 5–13.5 m (Zhu, 2007). These mudstones, carbonaceous-mudstones and coals have TOC values varying from 0.4% to 98.5%, Rock-Eval S_1+S_2 values ranging between 0.5 and 143 mg/g TOC (Fig. 7). The recent drilling in the deepwater area reveals that the Yacheng Formation is coal-bearing here as well and was deposited in coastal plain and littoral to neritic depositional environments; the potential source rocks include black shales, carbonaceous shales and coals, leading to a wide range of TOC values (shale: 0.4%–1.6%, carbonaceous shale: 6.1%–21%) and varying Rock-Eval S_1+S_2 values similar to those of the Yacheng Formation in the shallow water areas, though there are few TOC-rich samples in the deepwater area (Fig. 7). Microscopic examination shows that the kerogens of the Yacheng Formation source rocks from both the deepwater and shallow water areas contain 60–95% of vitrinite and inertinite, and only 5–30% of amorphous organic matter (Fig. 8). It is worth noting that the vitrinite and inertinite maceral content is reduced from the Lower Oligocene Yacheng Formation to the Upper Oligocene Lingshui Formation due to the change in their depositional environments. As illustrated by the sedimentary facies in Fig. 8, the Yacheng Formation is formed in a transitional coastal plain and tidal-flat environment with a large terrestrial input, resulting in the predominance of vitrinite and inertinite macerals; in contrast, the Lingshui Formation is deposited mainly in a shallow marine environment with reduced terrestrial input and increased planktonic input, resulting in increased exinite and even the appearance of amorphous organic matter in the kerogen. These geochemical and petrological data indicate that the Yacheng Formation source rocks are enriched in higher plant-derived organic matter that contains mainly gas-prone types II_b and III kerogens.

The Eocene shale of Wenchang Formation in the adjacent Pearl River Mouth Basin is believed to be one of the main source rocks in that area, with a total thickness of several hundred meters (Huang et al., 2003a; Zhu et al., 2009). These shales have TOC values ranging between 0.65% and 5.22% with oil-prone types II_a and I kerogens (Huang et al., 2003a; Zhu et al., 2009). Their distinctive biomarker features are relatively high abundance of C_{30} 4-methylsteranes (Huang et al., 2003a; Zhu et al., 2009; Cheng et al., 2012), a biomarker commonly distributed in Cenozoic lacustrine sediments in eastern China (Brassell et al., 1988; Ji et al., 2011) and probably biologically related to certain dinoflagellates thriving in freshwater lakes (Fu et al., 1990; Ji et al., 2011). This type

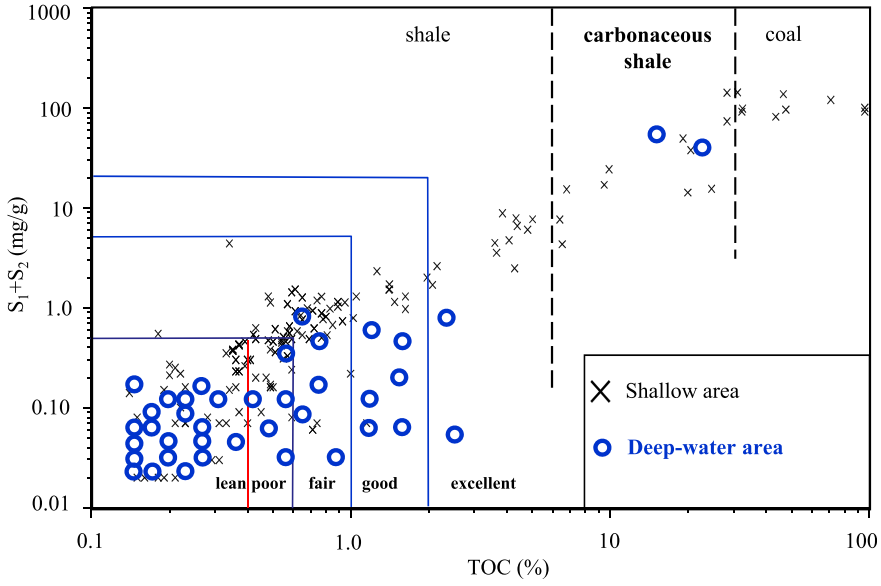

Fig. 7. Crossplot of TOC vs. Rock-Eval S_1+S_2 values for potential gas source rocks in the Oligocene Yacheng Formation.

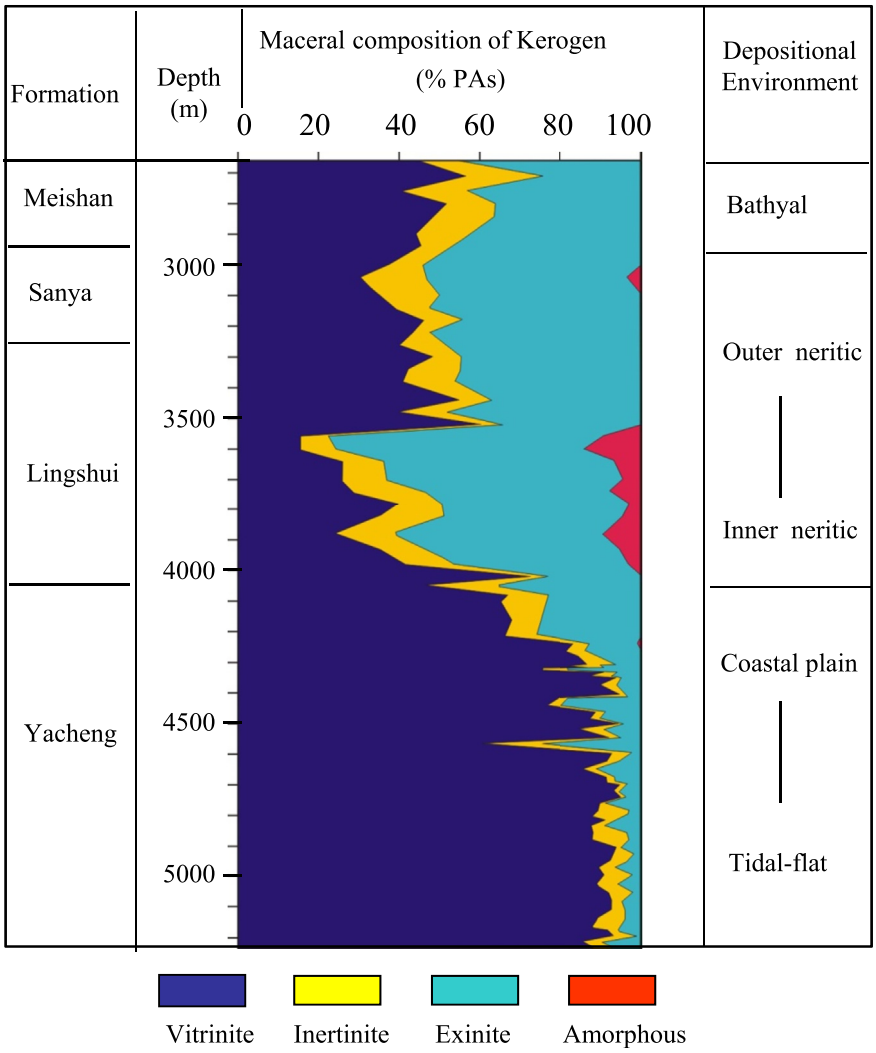

Fig. 8. Maceral composition profile of kerogens isolated from mudstone samples for the well SS191in the deepwater area. The Yacheng Formation source rocks are dominated by vitrinite. % PAs = Particle abundances of individual macerals.

of source rock has not been penetrated in the Qiongdongnan Basin possibly due to their absence in uplifts, but Zhu et al. (2009) reported that the oil-bearing sands from the well BD1531 contain relatively high abundance of C_{30} 4-methylsteranes in the *m*/*z* 217 and *m*/*z* 231 mass chromatograms. These C_{30} 4-methylsteranes are identified commonly in the Eocene lacustrine source rocks in the Pearl River Mouth and Beibuwan basins (Huang et al., 2003a, 2013), implying that Eocene source rocks are also present in the central depression of the Qiongdongnan Basin with uncertain hydrocarbon potentials.

To reconstruct the burial and thermal maturation history of Yacheng Formation source rocks, two pseudo-wells are created in the Lingshui Sag, with pseudo-well C in the central sag and pseudo-well D in the slope area nearby the SS17-2 gas field (Fig. 1b). The 1D burial history was reconstructed using the Integrated Exploration System software by back-stripping the present day sedimentary thickness of each stratigraphic unit in time and taking into account of thickness changes by compaction (Yahi et al., 2001; Brandes et al., 2008). The compaction model in IES software is based on that the compressibility of a rock relates to its lithology. The petrophysical properties of a rock unit that contain multiple lithologies, including density, initial porosity, permeability, compressibility coefficient, thermal conductivity and heat capacity, are automatically calculated by the software by weighing each pure or default lithology (sandstone, shale, limestone, etc.) according to its relative proportion in the rock unit (Yahi et al., 2001). The main inputs for the 1D burial history include: (1) the ages of each stratigraphic unit listed in Fig. 2 and Table 3; (2) the thickness of individual stratum that can be obtained from well data for shallow strata and from seismic data from deep strata when well data are not available; (3) the lithology of individual stratum that can be read from the neighbor wells and/or wells in shallow water areas by assuming that the lithological characteristics of rocks formed

Table 3
Input paleo-geothermal data for pesudo-wells C and D.

Stratigraphic unit	Age(Ma)	Paleo-geothermal gradient (°C/100 m)
Q	1.9–0	4.34
Pliocene YGH Fm.	5.5–1.9	3.7–3.9
Upper Miocene HL Fm.	10.5–5.5	3.7
Middle Miocene MS Fm.	16.5–10.5	3.7–3.8
Lower Miocene SY Fm.	23–16.5	3.8
Upper Oligocene LS Fm.	30–23	3.6–3.9
Lower Oligocene YC Fm.	33.9–30	3.6
Eocene-Paleocene	65–33.9	3.4–3.5

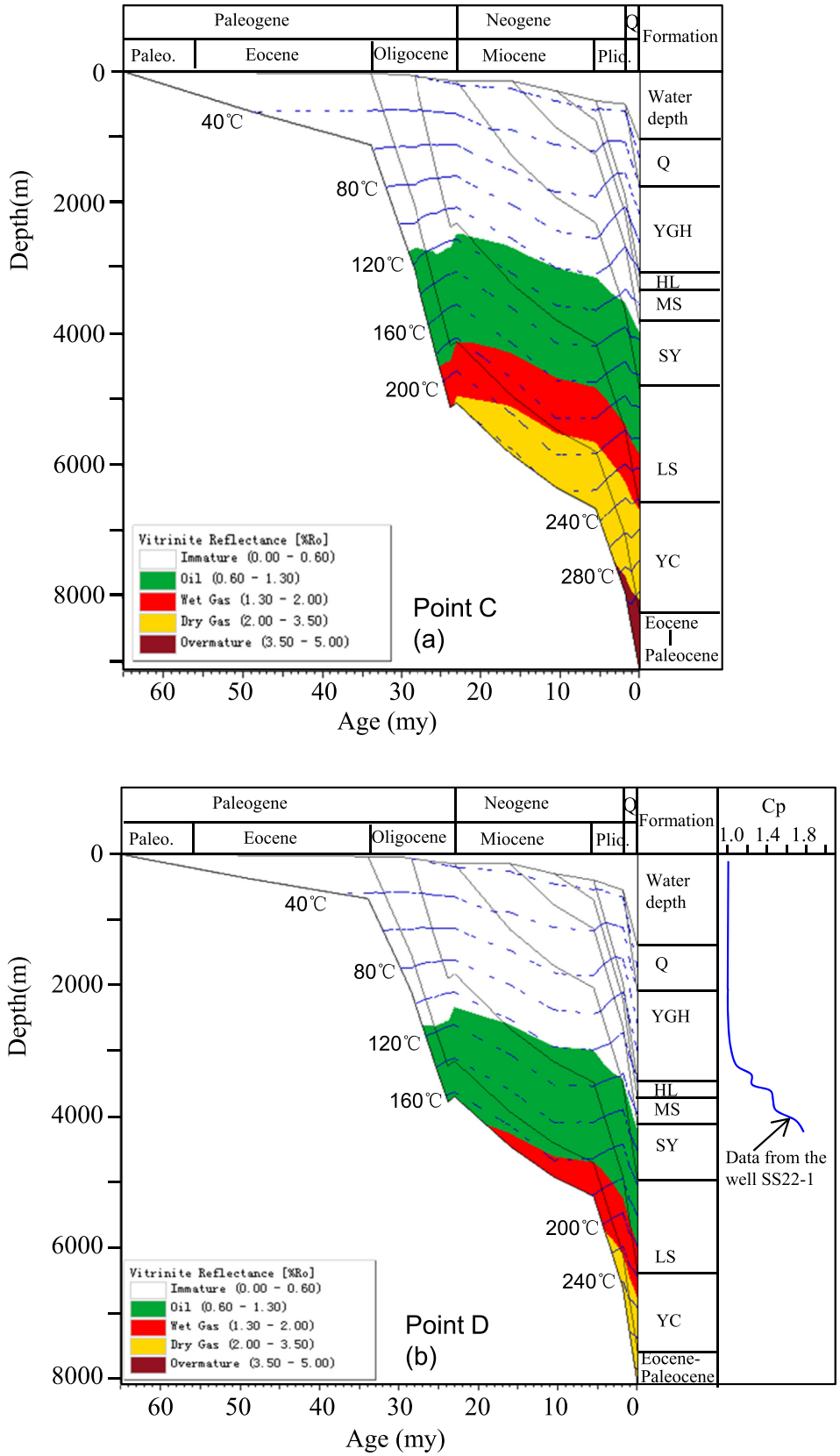

Fig. 9. Burial and thermal history of the strata for the pseudo-wells in the Lisngshui Sag of Qiongdongnan Basin. Pseudo-well C is close to the depocenter of Lingshui Sag and Pseudo-well C is near the gas fields (see Fig. 1b). Abbreviations: YGH-Yinggehai Formation; HL-Huangliu Formation; MS-Meishan Formation; SY-Sanya Formation; LS-Lingshui Formation; YC-Yacheng Formation; Cp: formation pressure coefficient, the ratio of measured pore fluid pressure to hydrostatic pressure.

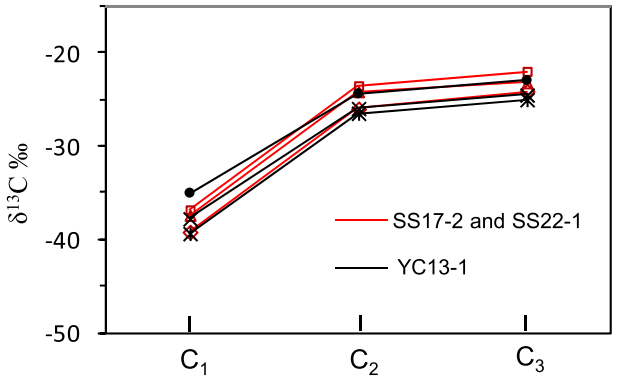

Fig. 10. Carbon isotopic fingerprint curves of natural gases showing the relationships between the gases from the SS17-2 and SS22-1(deep water area) and the YC13-1(shallow water area) gas fields.

under similar depositional environments should be identical and comparative; and (4) the paleo-water depth during various depositional periods that can be estimated by available microfossils and depositional facies.

The average current geothermal gradient is about 3.9–4.5°C/100 m in the deep-water area (approximately 3.9–4.34°C/100 m in the Lingshui Sag) of the Qiongdongnan Basin (Zhu et al., 2009; Huang et al., 2012) and the current burial depth of the Yacheng Formation ranges from 4000 to 7000 m (Fig. 8a). Based on the measured thermal conductivity of rocks, present geothermal gradient and sea floor heat flow, Shi et al. (2003, 2014) and Wang et al. (2014) investigated the geothermal evolution in the deep-water area of Lingshui Sag using the rifting heat flow model (McKenzie, 1978) and suggested that the paleo-geothermal gradient was 3.45–3.6 °C/100 m during the early rifting stage (65–34 Ma), 3.6–3.9 °C/100 m during the late rifting stage (34–23 Ma), 3.8–3.6 °C/100 m during the post-rift stage (23–5.5Ma) and 3.7–4.34 °C/100 m in the last rapid subsidence since 5.5Ma (Table 3). Using these parameters as initial inputs, the thermal maturation of source rocks for the two pseudo-wells were reconstructed using the EasyRo% model (Sweeney and Burnham, 1990); and the pseudo-well D that is close to the gas field was calibrated by measured vitrinite reflectance data when they are available from neighbor wells.

The 1D basin modeling results show that the Yacheng source rocks in the depocenter of Lingshui Sag reached peak of gas generation during Miocene to Pliocene (Fig. 9a) and the main gas window for those nearby the Central Canyon System occurred even later (Fig. 9b). It is the good match between the gas generation peak and the timing of trap formation that provides favorable conditions for the large-scaled accumulation of natural gas. The Eocene source rock has a current burial depth exceeding 6000 m in the depositional center of the sags and is within thermal stage of oil-cracking (Zhu et al., 2009; Huang et al., 2015), providing another possible gas supply.

4.3. Gas-source correlation

The chemical and stable carbon isotopic compositions of a gas are useful for identifying its sources (Schoell, 1984; Santos and John, 1999). Recently, the carbon isotopic fingerprinting correlation of gases has been integrated with other geochemical parameters to enhance the accuracy of source assignments (Mayer et al., 2007). The carbon isotopic compositions of the wet gases, such as ethane, propane, butane and isobutane, can reflect their sources as well as maturities, and they are less affected by migration as compared to methane, thus particularly valuable for correlating gases from different reservoirs (James, 1983). As shown in Table 1, all of the gases from both the SS17-2 and YC13-1 fields are similar in their isotopic and compositional data regardless of their reservoir age, except their variable amounts of non-hydrocarbon gases (CO_2 and N_2). The similarity of the gases from the two gas fields becomes more apparent from their carbon isotopic fingerprinting curves (Fig. 10), indicating they have probably originated from source rocks with similar depositional facies. Previous studies illustrated that the hydrogen isotopic compositions of gases can be used to evaluate the paleoenvironments of their source rocks (Yeh and Epstein, 1981; Schoell, 1984; Norville and Dawe, 2007). The D_{CH4} values of the SS22-1 gases range from −145 to −147‰ and are similar to those of the YC13-1 gases that are derived from the Oligocene coal-bearing Yachneg Formation in the Yanan Sag.

Small amounts of condensates associated with the gases were obtained from the SS17-2 gas filed. These condensates are of low density (0.8183 g/cm^3) and low wax content (1.42%). Their high pristane/phytane ratios (3.0–4.1) are similar to those of oils derived from terrestrial source rocks in the Tarim Basin (Li et al., 1999) and Pearl River Mouth Basin (Huang et al., 2003a) in China and the Gippsland Basin in Australia (Philp and Gilbert, 1986). These gas-associated condensates are also characterized by abundant oleanane and bicadinanes, diagnositic biomarkers for terrigenous organic matters widely distributed in the Tertiary strata of Southeastern Asia (Cox et al., 1986; van Aarssen et al., 1990), in the condensates of YC 13-1 gas field and the coastal plain source rocks in the Oligocene Yacheng Formation (Fig. 11). Compared with the YC1316 condensates sourced from the carbonaceous shales of Yacheng Formation, the SS17-2 condensates contain relatively low abundance of bicandinaes derived from specific angiosperm resins (van Aarssen et al., 1992), but has a better correlation with the neritic shales of Yacheng Formation (Fig. 11), implying the reduced inputs of terrigenous angiosperm plants toward the centers of sags during the deposition period of Yacheng Formation.

Based on the above discussions, it is believed that the natural gases in the SS17-2 and SS22-1 gas fields in the deepwater area are derived from the underlying Yacheng Formation in the Lingshui Sag deposited under neritic pro-delta environments with predominant inputs of terrestrial organic matter.

4.4. Timing of gas accumulation

Coupled with detailed burial history, the homogenization temperatures of oil and coeval aqueous fluid inclusions have been widely used to investigate the charging time of oil reservoirs (Karlsen et al., 1993; Gan et al., 2009). However, dating the migration and accumulation of gases by this method is difficult since petroleum inclusions are rarely present in gas reservoirs (Xiao et al., 2002). Recently, the combination of isotope-specific reaction kinetics with burial history models has proved to be a useful tool to date gas migration and accumulation (Tang et al., 2000; Cramer et al., 2001; Xiao et al., 2006). Based on the gas yields and $\delta^{13}C$ values of methane generated from the Yacheng Formation source rock during pyrolysis at two heating rates of 2 °C/h and 20 °C/h, the kinetic parameters of methane carbon isotope fractionation are calculated using the method of Tang et al. (2000) and listed in Table 2. These kinetic parameters were used to reconstruct the history of gas generation and methane carbon isotope fractionation through geological time based on the burial and thermal histories of the pseudo-well D as discussed in section 4.2 (Fig. 9b). As illustrated in Fig. 12a, the rapid gas generation from Yacheng Formation source rocks near the Central Caynon System began after 5Ma. The methane isotopic composition of gases in the reservoir depends on not only their sources, but also their accumulation models, i.e,

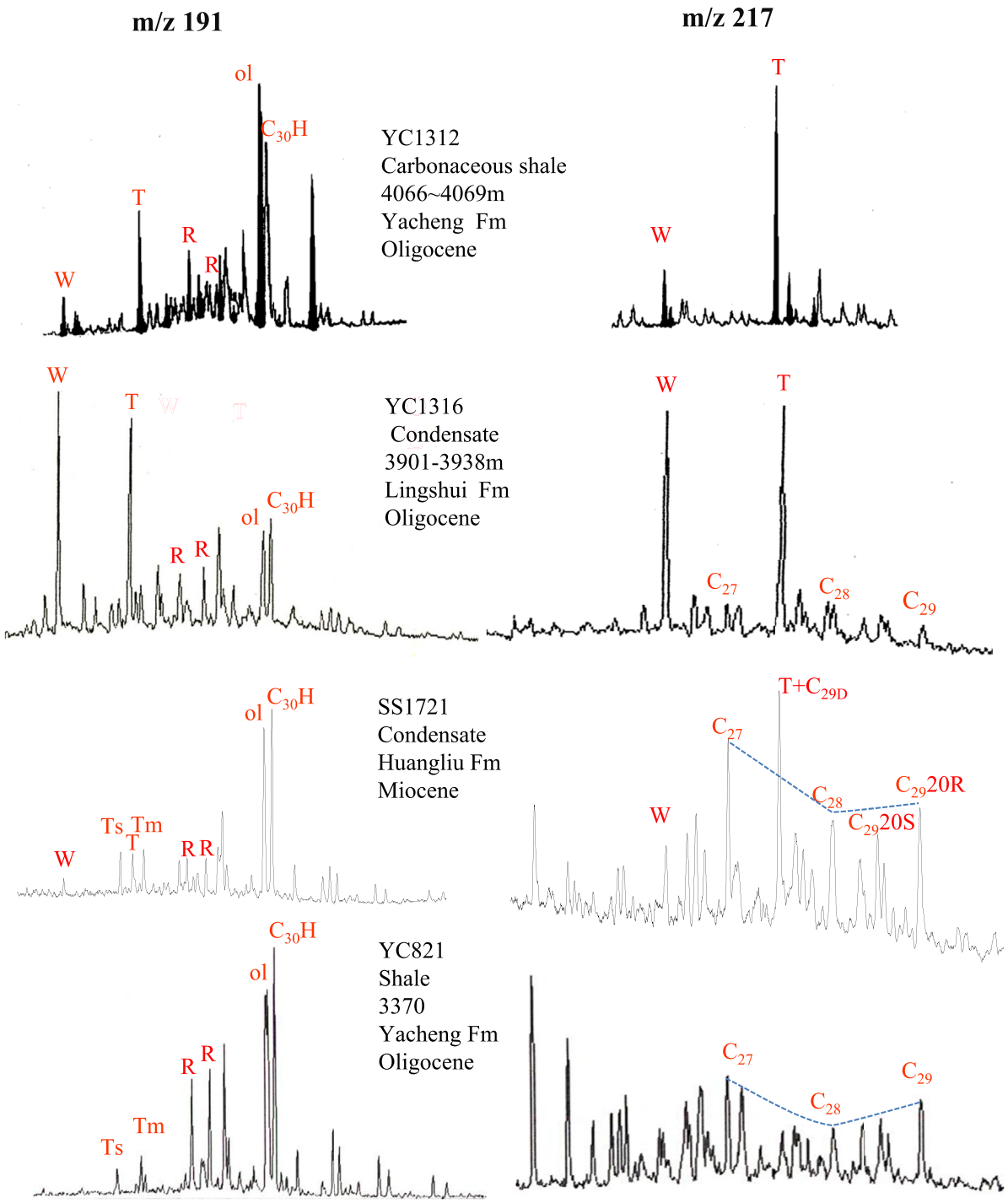

Fig. 11. Representative *m/z* 191 and 217 mass fragments showing the correlation between the condensates and potential source rocks. W, T and R: bicadinanes; ol: oleanane; Ts:18α(H)-22,29,30-trisnorneohopane; Tm: 17α(H)-22,29,30-trisnorhopane; C_{29D}: 13α(H), 17β(H) −20(S)-24-ethyl-cholestane (diasterane); C_{27}, 5α(H),14α(H),17α(H)-20(R)-cholestane; C_{28}, 5α(H),14α(H),17α(H)-20(R)-24-methyl-cholestane; C_{29}(C_{29}20R), 5α(H),14α(H),17α(H)-20(R)-24-ethyl-cholestane; C_{29}20S, 5α(H),14α(H),17α(H)-20(S)-24-ethyl-cholestane.

cumulative or instant accumulation (Rooney et al., 1995). The instant and cumulative carbon isotope of the methane generated from this gas kitchen is −34.7‰ and −39.8‰, respectively (Fig. 12b). The stable carbon isotopes of methane in the SS17-2 and SS22-1gas fields are in the range of −39.4‰ to −36.8‰, indicating that they are neither cumulative nor instantaneous, but partially cumulative. As mentioned above, the SS17-2 and SS22-1 gas reservoirs are very young and the effective traps were developed after 4 Ma, indicating that no gases generated earlier than 4Ma can be preserved in the present gas pool. Following the method of Rooney et al. (1995), the carbon isotopes of methane generated after 4 and 3Ma were calculated respectively and founded to be well matched with the carbon isotopes of reservoired methane (Fig. 12b), implying that the effective gas accumulation began when the effective traps were formed around 4Ma. Nevertheless it should be kept in mind that this method is only tentative to infer the gas

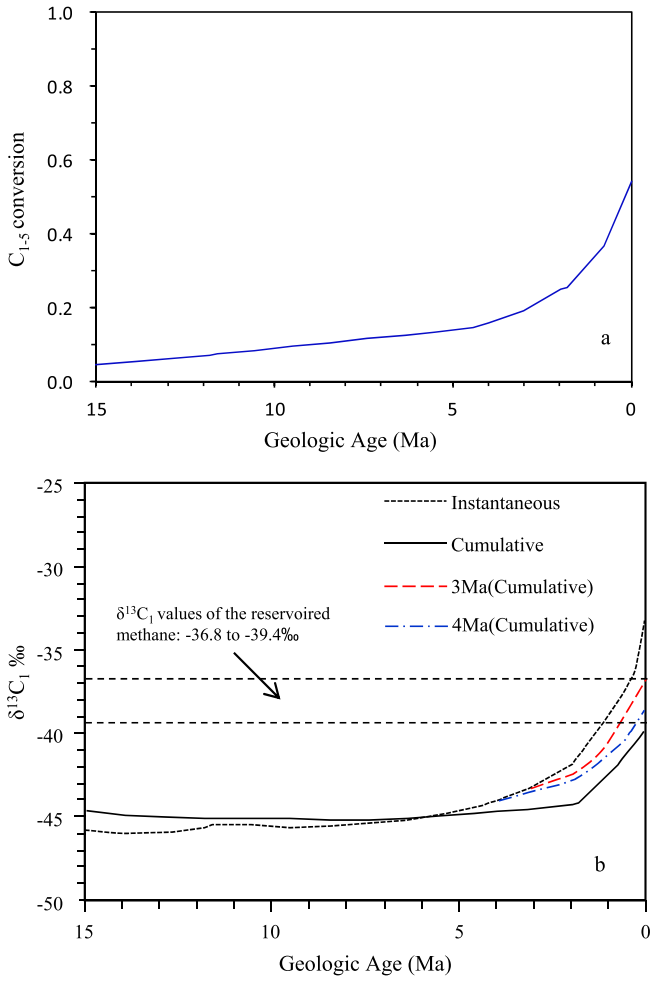

Fig. 12. Reconstructed gas generation (a) and methane carbon isotope fractionation curves (b) of methane from the Yacheng Formation source rocks near the Central Canyon System (point D shown in Fig. 1b and Fig. 13), showing that the measured $\delta^{13}C_1$values of the reservoired gases ranging from −39.4 to −36.8‰ are well matched with the $\delta^{13}C_1$ of methane accumulated since 3 or 4 Ma. See details in text.

formation time because the source rocks may have different stable isotopic values due to their variation in depositional environments, which in turn affects the carbon isotopes of reservoired methane. Therefore, further efforts are still needed to more accurately investigate the gas charging time by fluid inclusions in the future.

4.5. Gas accumulation model and implications for petroleum exploration

As discussed above, the natural gases in the SS17-2 and SS22-1 gas fields originate from the underlying Yacheng Formation source rocks in the Lingshui Sag. The gas migration model is illustrated in Fig. 13. Mud diapirs and faults might have acted as pathways for upward gas migration since they connects the source rocks with the upper sandy carrier beds and unconformities. The sandstones deposited on the unconformities may have been the preferable conduits for lateral gas migration. The most common forces influencing gas migration are buoyancy and pressure differential in the Lingshui Sag. While the buoyancy-driven gas migration is common in shallower, normally pressured reservoirs, it might be minor in overpressured intervals where large-scale gas migration with commercial quantities is most likely related to large pressure gradients (Lee and Williams, 2000; Webster et al., 2011). Significant overpressure is encountered in the nearby well SS221 (Fig. 9b). The formation pressure coefficient (Cp) is less than 1.2 in sandstone reservoirs at a depth of less than 3300 m, indicating an almost hydrostatic pressure system. The strong overpressure zone (Cp > 1.6), however, is encountered at a depth greater than 4000 m in Meishan and Sanya Formations (Fig. 9b) and the Cp value is predicted to be as high as 2.10 in the Yacheng Formation source rock layers (Zhu et al., 2011). Overpressures developed in the source rocks in central basin appear to be the main driving-force for fluid migration (Xie et al., 2001). Notably, the diapiric structures (intermittently chaotic and blank seismic reflections) like those in Yinggehai Basin are also observed in the area (Fig. 3), and the deep source rocks in the Yacheng Formation are cut through by the mud diapirs/faults along which the gases migrate vertically to Pliocene reservoirs.

Although the SS17-2 and SS22-1 gas fields are young with their traps being formed until the development of sealing rocks in the

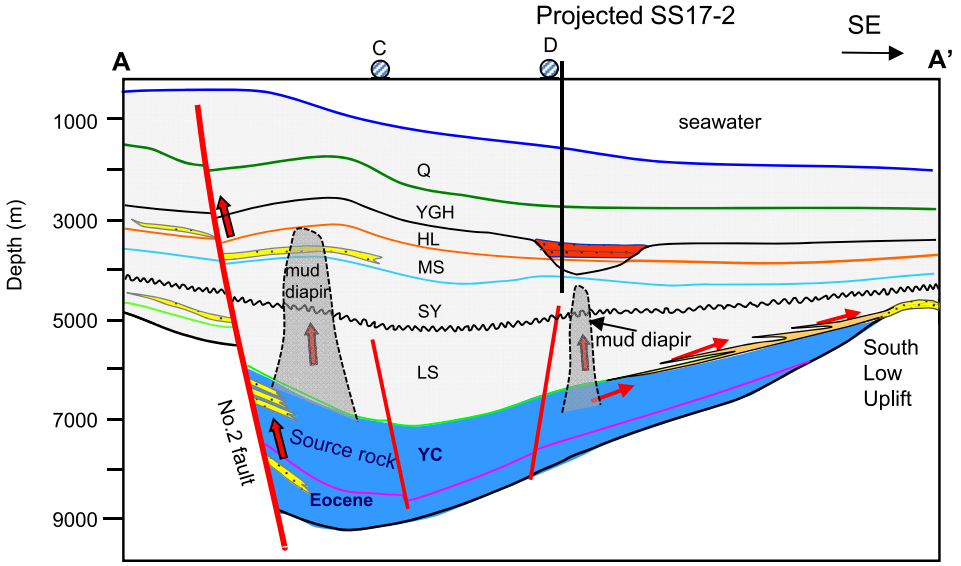

Fig. 13. Gas migration pathways and accumulation model in the Lingshui Sag of Qiongdongnan Basin, illustrating that faults and gas chimneys as gas pathways. The Formation abbreviations are the same as in Fig. 9. The location of the section is shown in Fig. 1b, and points C and D indicate the pseudo-wells in Figs. 9 and 12.

lower part of Yinggehai Formation (early Pliocene), it is possible for the gases to accumulate on a large scale within a very short time span because the gas migration was driven by high pressure with high gas expulsion efficiencies. This also implies that the sags in the deepwater area of this basin may contain abundant natural gas resources and the central submarine canyon system possesses the most favorable conditions for a gas play, including the proximity to gas source kitchen, the development of suitable reservoirs with good permeability and the diapirs/faults migration conduits. In addition, both the South Low Uplift and the No.2 Fault zone in the deep-water area are on the pathways of upward- or lateral gas migration (Fig. 13), therefore they should be also favorable places for gas accumulation.

5. Conclusions

(1) The gases from the deepwater area of the Qiongdongnan Basin are dominated by hydrocarbon gases with 91.2–92.9% methane and 5.9–7.5% C_{2+} hydrocarbons with 0.78–3.09% nonhydrocarbon gases (N_2 and CO_2) and characterized by $\delta^{13}C_1$ values of −36.8‰ to −39.4‰, $\delta^{13}C_2$ values of −23.5‰ to −26.2‰ and δD_{CH4} values of −144‰ to −147‰. The gases are generated from humic type source rocks with high maturities. The low CO_2 content of less than 1% by volume and their carbon isotope ranges of −20.7‰ to −8.5‰ in the gases from the SS17-2 and SS22-1 gas fields reveal that they are of organic origins, thus implying that the risk of CO_2-rich gas could be greatly reduced in the deepwater area far away from the No. 2 Fault.

(2) Gas-source correlation results indicate that the gases in the deepwater area most likely originate from the humic organic matter in the Oligocene Yacheng Formation source rocks and accumulate through vertical migration from the deeply buried source kitchen in the Lingshui Sag.

(3) The gas charging of the SS17-2 gas field occurred very late, mainly from 3 or 4 Ma to present day based on the trap formation time and the methane generation model. Mud diapirs and faults act as the main pathways for the upward gas migration from deep kitchens, and the sandstones formed on the unconformities are favorable conduits for lateral migration. The reconstructed gas migration model has a significant implication that the future hydrocarbon exploration in the deepwater area should be focused on the Central Canyon System, the South Low Uplift and the zones near No.2 Fault.

Acknowledgments

We are grateful to Prof. Nicholas Harris and two anonymous reviewers for constructive comments that improved the clarity of this manuscript significantly. The authors are indebted to CNOOC China Ltd, Zhanjiang Branch for providing us with gas, condensate and source rock samples and making available the seismic data. This work was financially supported by National Science and Technology Major Project of China (Grant No. 20011ZX05025-002 and 2016ZX05026002-005). This is contribution No. IS-2191 from GIGCAS.

References

Brandes, C., Astorga, A., Littke, R., Winsemann, J., 2008. Basin modelling of the Limón Back-arc Basin (Costa Rica): burial history and temperature evolution of an island arc-related basin-system. Basin Res. 20, 119–142.

Brassell, S.C., Sheng, G., Fu, J., Eglinton, G., 1988. Biological markers in lacustrine Chinese oil shales. In: Fleet, A.J., Kelts, K., Talbot, M.R. (Eds.). Lacustrine Petroleum Source Rocks, Blackwell, pp. 299–308.

Chen, H., Li, S., Sun, Y., Zhang, Q., 1998. Two petroleum systems charge the YA13-1 gas field in Yinggehai and Qiongdongnan Basins, South China Sea. AAPG Bull. 82, 757–772.

Cheng, P., Xiao, X.M., Tian, H., Huang, B.J., Wilkins, R.W.T., Zhang, Y.Z., 2012. Source controls on geochemical characteristics of crude oils from the Qionghai uplift in the western Pearl River Mouth Basin, offshore South China Sea. Mar. Pet. Geol. 40, 85–98.

Cox, H.C., De Leeuw, J.W., Schenk, P.A., van Koningsveld, H., Jansen, J.C., van De Graaf, B., van Geerestein, V.J., Kanters, J.A., Kruk, C., Jans, A.W.H., 1986. Bicadinane, a C_{30} pentacyclic isoprenoid hydrocarbon found in crude oil. Nature 319, 316–318.

Cramer, B., Krooss, B.M., Littke, R., 1998. Modeling isotope fractionation during primary cracking of natural gas: a reaction kinetic approach. Chem. Geol. 149, 235–250.

Cramer, B., Faber, E., Gerling, P., Krooss, B.M., 2001. Reaction kinetics of stable carbon isotopes in natural gas–insights from dry, open system pyrolysis experiments. Energy Fuels 15, 517–532.

Dai, J., 1993. Carbon and hydrogen isotope characteristics of natural gas and identification of various genetic gases. Nat. Gas. Geosci. 4, 1–40 (in Chinese with English Abstract).

Dai, J.X., Song, Y., Dai, C.S., Wang, D.R., 1996. Geochemistry and accumulation of carbon dioxide gases in China. AAPG Bull. 80, 1615–1626.

Fu, J., Sheng, G., Xu, J., Eglinton, G., Gower, A.P., Jia, R., Fan, S., Peng, P., 1990. Application of biological markers in the assessment of paleoenvironments of Chinese non-marine sediments. Org. Geochem. 16, 769–779.

Gan, H.J., Tian, H., Huang, B.J., Wilkins, R.W.T., Tang, Y.C., Xiao, X.M., 2009. Generation and accumulation of oil and condensates in the wenchang a sag, western Pearl River mouth Basin, South China sea. Geofluids 9, 275–286.

Gong, Z.S., Li, S., 1997. Continental margin Basin Analysis and Hydrocarbon Accumulation of the Northern South China Sea. Science Press, Beijing, p. 458 (in Chinese).

Gong, C.L., Wang, Y.M., Zhu, W.L., Li, W.G., Xu, Q., Zhang, J.M., 2011. The central submarine canyon in the Qiongdongnan Basin, northwestern South China Sea: architecture, sequence stratigraphy, and depositional processes. Mar. Pet. Geol. 28, 1690–1702.

Hill, R.J., Zhang, E., Katz, B.J., Tang, Y., 2007. Modeling of gas generation from barnett shale, Fort Worth Basin, Texas. AAPG Bull. 91, 501–521.

Huang, B.J., 1999. Gas potential and favorable exploration area in the Qiongdongnan Basin. Nat. Gas. Ind. 19, 26–32 (in Chinese with English Abstract).

Huang, B.J., Xiao, X.M., Zhang, M.Q., 2003a. Geochemistry, grouping and origins of crude oils in the Western Pearl River Mouth basin, offshore South China Sea. Org. Geochem. 34, 993–1008.

Huang, B.J., Xiao, X.M., Li, X.X., 2003b. Geochemistry and origins of natural gases in the Yinggehai and Qiongdongnan basins, Offshore South China Sea. Org. Geochem. 34, 1009–1025.

Huang, B.J., Li, X.S., Wang, Z.F., Li, L., Huang, Y.W., 2012. Characteristics and gas generation potential of source rocks in the deepwater area, the Qiongdongnan basin. China Offshore Oil Gas 24, 1–7 (in Chinese with English Abstrract).

Huang, B.J., Tian, H., Wilkins, R.W.T., Xiao, X.M., Li, L., 2013. Geochemical characteristics, palaeoenvironment and formation model of Eocene organic-rich shales in the Beibuwan Basin, South China Sea. Mar. Pet. Geol. 48, 77–89.

James, A.T., 1983. Correlation of natural gas by use of carbon isotopic distribution between hydrocarbon components. AAPG Bull. 67, 1176–1191.

Ji, L.M., Meng, F.W., Yan, K., Song, Z.G., 2011. The dinoflagellate cyst Subtilisphaera from the Eocene of the Qaidam Basin, northwest China, and its implications for hydrocarbon exploration. Rev. Palaeobot. Palynol. 167, 40–50.

Karlsen, D.A., Nedkvitne, T., Larter, S.R., 1993. Hydrocarbon composition of authigenic inclusions: application to elucidation of petroleum reservoir filling history. Geochim. Cosmochim. Acta 57, 3641–3659.

Lee, M., Williams, D.D., 2000. Paleohydrology of the Delaware Basin, Western Texas: overpressure development, hydrocarbon migration, and ore genesis. AAPG Bull. 84, 961–974.

Leythaeuser, D., Schaefer, R.G., Cornford, C., 1979. Generation and migration of light hydrocarbon (C_2-C_7) in sedimentary basin. Org. Geochem. 10, 191–204.

Li, M., Lin, R., Liao, Y., Snowdon, L.R., Wang, P., Li, P., 1999. Organic geochemistry of oils and condensates in the Kekeya field, southwest depression of the Tarim Basin (China). Org. Geochem. 30, 15–37.

Mayer, B., Klassen, P., Cheung, K., Taylor, S.W., 2007. Isotopic fingerprinting of hydrocarbon gases from Cretaceous coalbeds and shallow aquifers of central Alberta, Canada. Geophys. Res. Abstr. Eur. Geosci. Union 2007 9, 05819.

McKenzie, D., 1978. Some remarks on the development of sedimentary basins. Earth Planet. Sci. Lett. 40, 25–32.

Norville, G.A., Dawe, R.A., 2007. Carbon and hydrogen isotopic variations of natural gases in the southeast Columbus basin offshore southeastern Trinidad, West Indies – clues to origin and maturity. Appl. Geochem. 22, 2086–2094.

Oxburgh, E.R., O'Nions, R.K., Hill, I.R., 1986. Helium isotopes in sedimentary basins. Nature 324, 632–635.

Philp, R.P., Gilbert, T.D., 1986. Biomarker distributions in Australian oils predominantly derived from terrigenous source material. Org. Geochem. 10, 73–84.

Rooney, M.A., Claypool, G.E., Chung, H.M., 1995. Modeling thermogenic gas generation using carbon isotope ratios of natural gas hydrocarbons. Chem. Geol. 126, 219–232.

Ru, K., Pigott, J.D., 1986. Episodic rifting and subsidence in the South China Sea. AAPG Bull. 70, 1136–1155.

Santos, N.E.V., John, M.H., 1999. Use of hydrogen and carbon stable isotopes

characterizing oils from the Potiguar Basin (Onshore), Northeastern Brazil1. AAPG Bull. 83, 496–518.
Schoell, M., 1983. Genetic characterization of natural gases. AAPG Bull. 67, 2225–2238.
Schoell, M., 1984. Recent advances in petroleum isotope geochemistry. Org. Geochem. 6, 645–663.
Shi, X.B., Qiu, X.L., Xia, K.Y., Zhou, D., 2003. Characteristics of surface heat flow in the South China Sea. J. Asian Earth Sci. 22, 265–277.
Shi, X.B., Wang, Z.F., Jiang, H.Y., Sun, Z.P., Yang, J., Yu, C.H., Yang, X.Q., 2014. Vertical variations of geothermal parameters in rifted basins and heatflow distribution features of the Qiongdongnan Basin. Chin. J. Geophys. 58, 939–952 (in Chinese with English abstract).
Su, M., Xie, X.N., Xie, Y.H., Wang, Z.F., Zhang, C., Jiang, T., He, Y.L., 2014. The segmentations and the significances of the central canyon system in the Qiongdongnan Basin, northern South China Sea. J. Asian Earth Sci. 79, 552–563.
Sweeney, J.J., Burnham, A.K., 1990. Evaluation of simple model of vitrinite reflectance based on chemical kinetics. AAPG Bull. 10, 1559–1570.
Tang, Y.C., Perry, J.K., Jenden, P.D., Schoell, M., 2000. Mathematical modeling of stable carbon isotope ratios in natural gases. Geochim. Cosmochim. Acta 64, 2673–2687.
Taylor, H., Teichmüller, M., Davis, A., Diessel, C.F.K., Littke, R., Robert, P., 1998. Organic Petrology. Borntraeger, Berlin-Stuttgart.
Tissot, B.P., Welte, D.H., 1984. Petroleum Formation and Occurrence, second ed. Springer-Verlag, Berlin.
van Aarssen, B.G.K., Cox, H.C., Hoogendoorn, P., de Leeuw, J.W., 1990. A cadinene biopolymer in fossil and extant dammar resins as a source for cadinanes and bicadinanes in crude oils from South East Asia. Geochim. Cosmochim. Acta 54, 3021–3031.
van Aarssen, B.G.K., Zhang, Q., de Leeuw, J.W., 1992. An unusual distribution of bicadinanes, tricadinanes and oligocadinanes in sediments from the Yacheng gasfleld, China. Org. Geochem. 18, 805–812.
Wang, P.R., Xu, G.J., Xiao, T.R., Zhang, D.J., Zhang, B., 2008. Application of C_5–C_{13} light hydrocarbons in depositional environment diagnosis. Prog. Nat. Sci. 18, 1129–1137 (in Chinese with English Abstract).
Webster, M., O'Connor, S., Pindar, B., Swarbrick, R., 2011. Overpressures in the Taranaki Basin: distribution, causes, and implications for exploration. AAPG Bull. 95, 339–370.
Xiao, X.M., Liu, Z.F., Liu, D.H., 2002. Fluid inclusions of reservoirs: application to studying of natural gas reservoir filling times. Chin. Sci. Bull. 47, 957–960.
Xiao, X.M., Xiong, M., Tian, H., Wilkins, R.W.T., Huang, B.J., Tang, Y.C., 2006. Determination of the source area of the Ya13-1 gas pool in the Qiongdongnan Basin, South China Sea. Org. Geochem. 37, 990–1002.
Xie, X., Bethke, C.M., Li, S., Liu, X., Zheng, H., 2001. Overpressure and petroleum generation and accumulation in the dongying depression of the Bohaiwan Basin, China. Geofluids 1, 257–271.
Xu, Y.C., Shen, P., 1996. A study of natural gas origins in China. AAPG Bull. 80, 1604–1614.
Yahi, N., Schaefer, R.G., Littke, R., 2001. Petroleum generation and accumulation in the Berkine Basin, Eastern Algeria. AAPG Bull. 85, 1439–1467.
Yeh, H.W., Epstein, S., 1981. Hydrogen and carbon isotopes of petroleum and related organic matter. Geochim. Cosmochim. Acta 45, 753–762.
Zhang, T., Zhang, M., Bai, B., Wang, X., Li, L., 2008. Origin and accumulation of carbon dioxide in the Huanghua depression, Bohai Bay Basin, China. AAPG Bull. 92, 341–358.
Zhu, W.J., 2007. Natural Gas Geology of Northern Part of South China Sea. Petroleum Industrial Press, Beijing (in Chinese).
Zhu, W.L., Huang, B.J., Mi, L., Wilkins, R.W.T., Fu, N., Xiao, X.M., 2009. Geochemistry, origin and deep-water exploration potential of natural gases in the Pearl River Mouth and Qiongdongnan Basins, South China Sea. AAPG Bull. 93, 741–761.
Zhu, J., Zhang, X., Zhang, G., Liu, F., Zhang, M., Chen, G., Xia, Y., 2011. A study of abnormal pressure distribution and formation mechanism in Qiongdongnan Basin. Nat. Gas. Geosci. 22, 324–330 (in Chinese with English Abstract).